Electronic Supplementary Material

Construction of CPs@MnO_2-AgNPs as multifunctional nanosensor for glutathione sensing and cancer theranostic

Qi Wang[a,b], Chunyan Wang[b], Xiaodong Wang[a], Yuan Zhang[a], Yuehuan Wu[b], Chuan Dong[a] and Shaomin Shuang[a,*]

[a] *College of Chemistry and Chemical Engineering, Institute of Environmental Science, Shanxi University, Taiyuan, 030006, PR China*

[b] *Chemistry & Chemical Engineering Department, Taiyuan Institute of Technology, Taiyuan, 030008, PR China*

*Corresponding author: smshuang@sxu.edu.cn (S. Shuang).

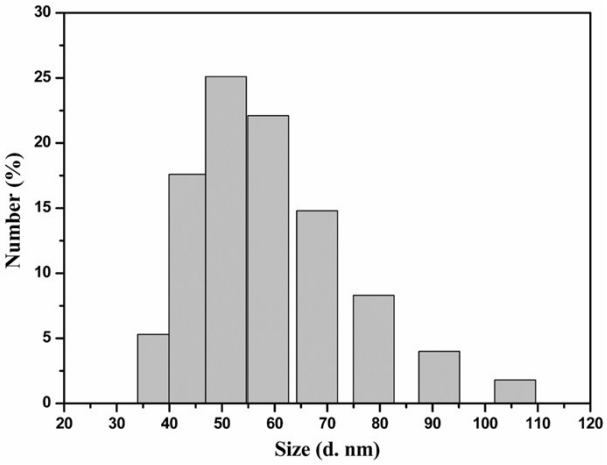

Fig. S1 Size distribution of as-prepared CPs.

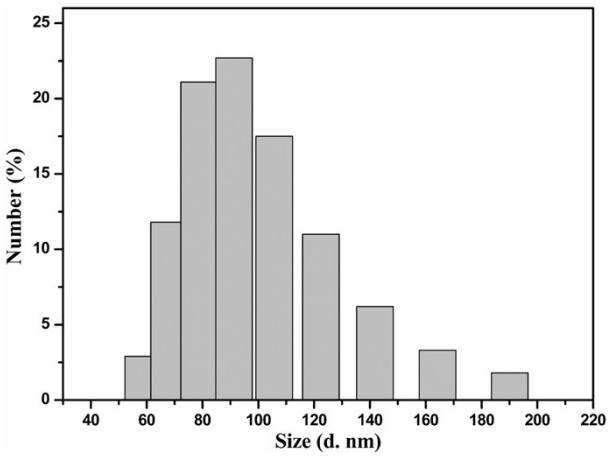

Fig. S2 Size distribution of as-prepared CPs@MnO_2 nanocomposite.

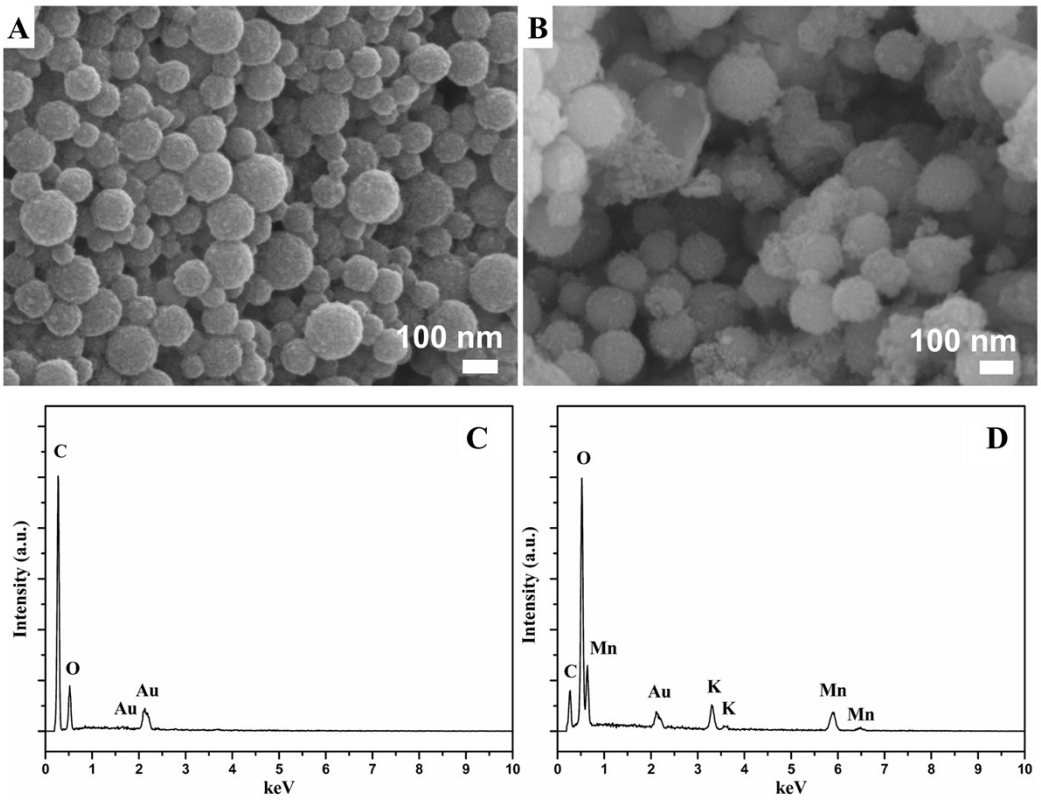

Fig. S3 SEM images of (A) CPs and (B) CPs@MnO_2 nanocomposite. EDS patterns of (C) CPs and (D) CPs@MnO_2 nanocomposite.

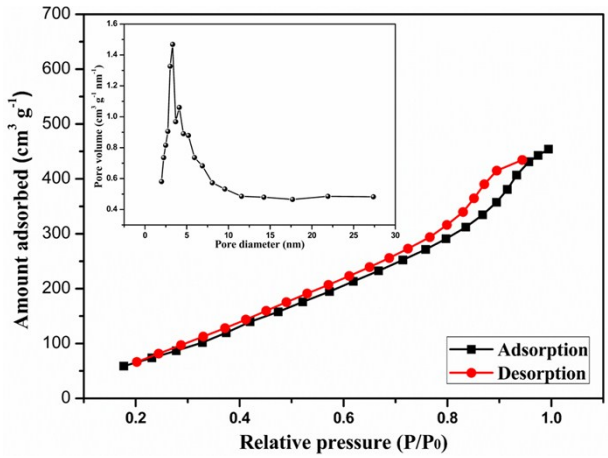

Fig. S4 The N_2 adsorption/desorption isotherms and pore-size distribution curve (inset) of as-prepared CPs@MnO_2 nanocomposite.

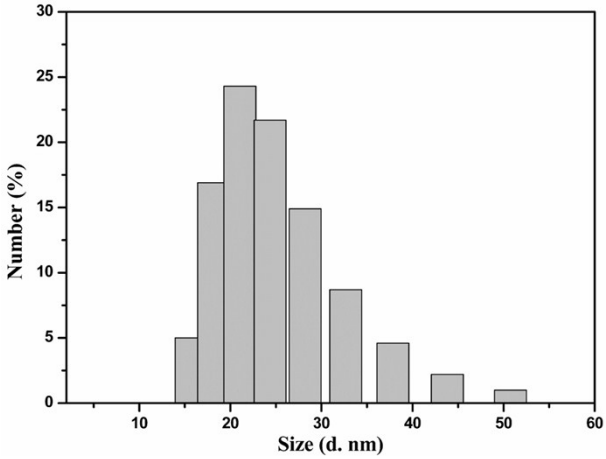

Fig. S5 Size distribution of as-prepared AgNPs.

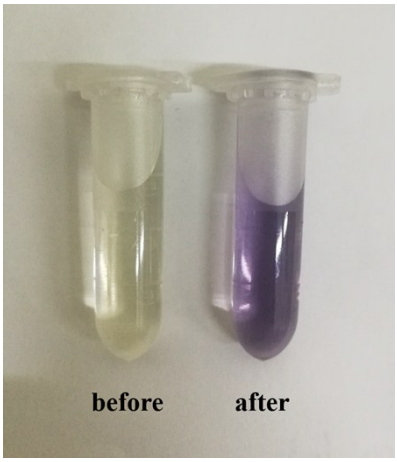

Fig. S6 The ninhydrin chromogenic reaction photos of CPs@MnO_2 before and after APTES capping.

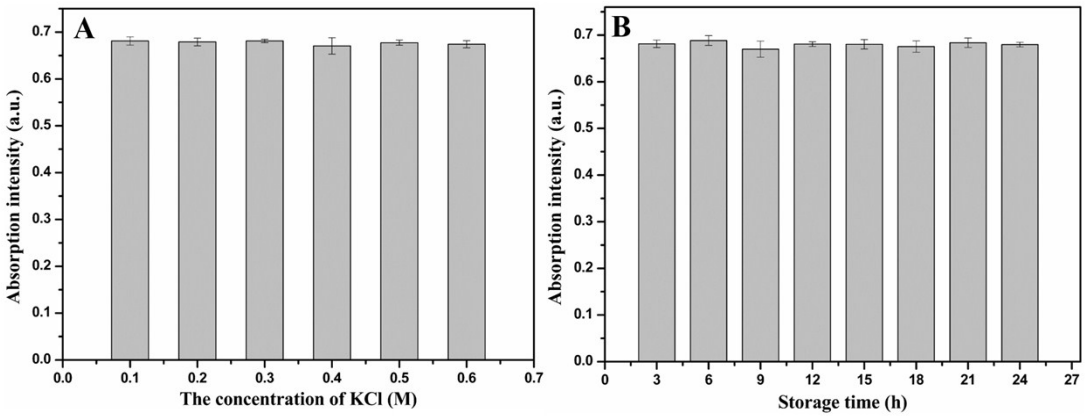

Fig. S7 The stability of CPs@MnO_2 (A) in different concentrations of KCl and (B) at different storage times.

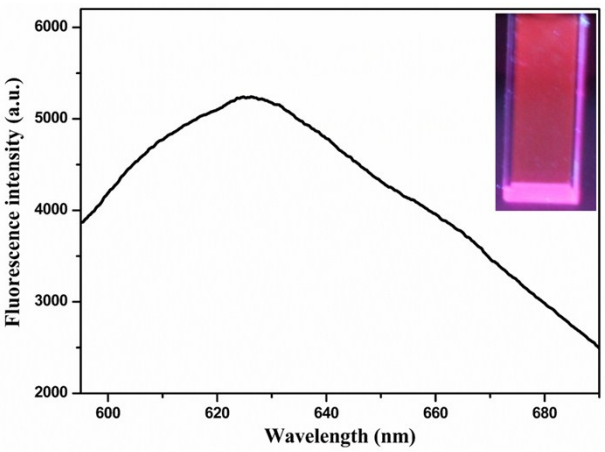

Fig. S8 The fluorescence emission spectrum of AgNPs. Inset: the photograph of AgNPs under UV light illumination.

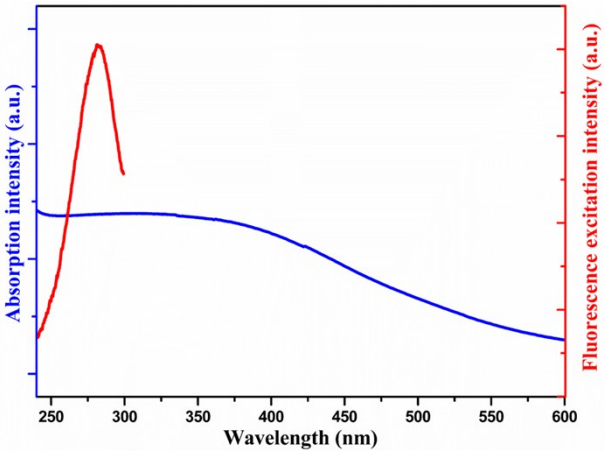

Fig. S9 The overlay of fluorescent excitation spectrum of Ag NPs and absorption spectrum of CPs@MnO_2.

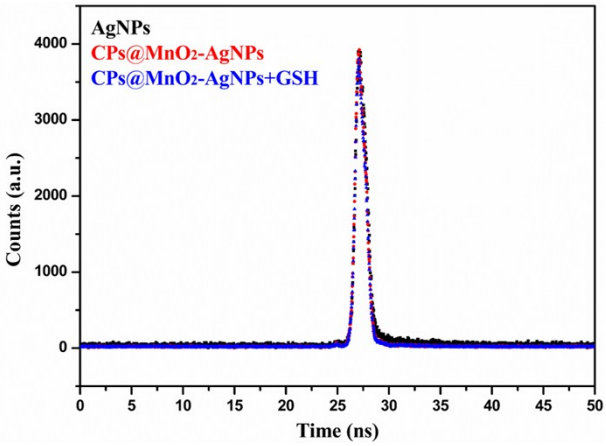

Fig. S10 Time-resolved fluorescence decay spectra at 630 nm from AgNPs, CPs@MnO_2-AgNPs

and CPs@MnO_2-AgNPs+GSH.

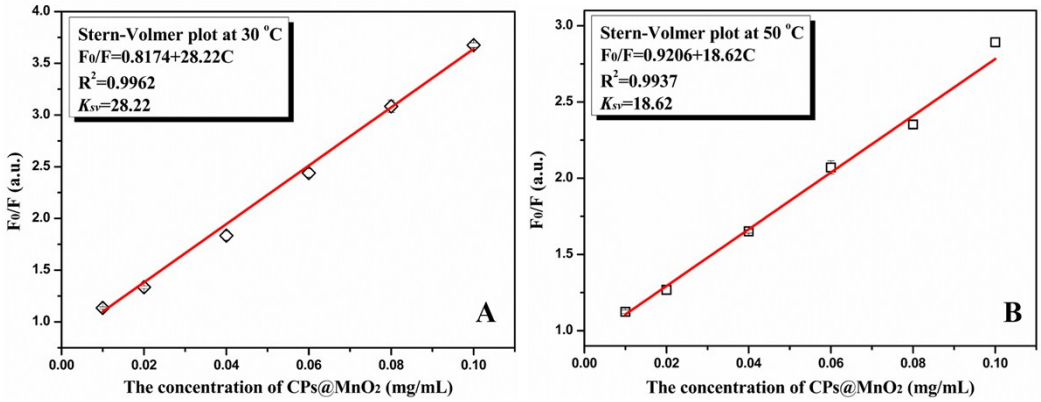

Fig. S11 Stern-Volmer plot describing the response of F_0/F to the CPs@MnO_2 nanocomposite concentration. F_0 is the fluorescence intensity of AgNPs, and F is the fluorescence intensity of AgNPs in the presence of CPs@MnO_2 nanocomposite.

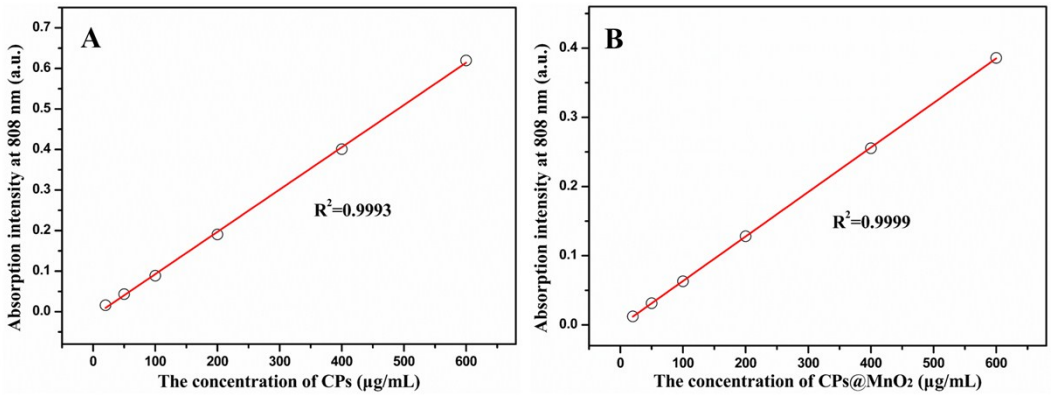

Fig. S12 The fitting curve of the absorbance of (A) CPs and (B) CPs@MnO_2 aqueous dispersions at 808 nm as a function of concentrations.

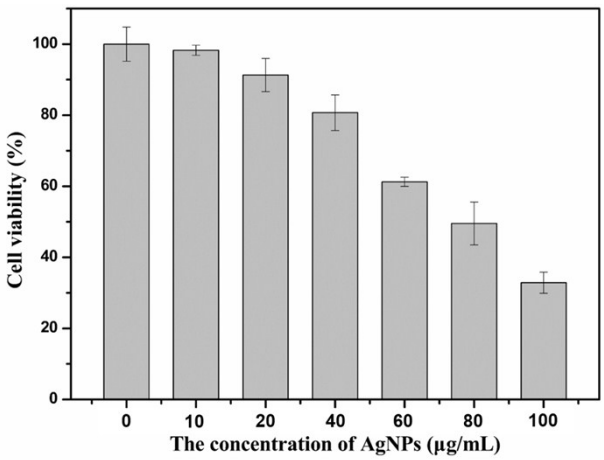

Fig. S13 Viability of SMMC-7721 cells after incubation with different concentrations of AgNPs for 24h.

Table S1 Parameters of multi-exponential fits to the fluorescence decay.

Species	τ_1 (ns)	τ_2 (ns)	B_1 (%)	B_2 (%)	χ^2	τ_{ave} (ns)
AgNPs	0.33	3.91	67.68	32.32	1.176	1.49
CPs@MnO_2-AgNPs	0.21	2.36	41.67	58.33	1.177	1.46
CPs@MnO_2-AgNPs+GSH	0.22	2.40	42.47	57.53	1.173	1.47

Table S2 Comparison of present method with reported methods.

Method	Detection limit (μM)	Linear range (μM)	Ref.
Eu^{3+} encapsulated carbon dots	0.05	0-50	7
Polydopamine NPs-MnO_2	1.5	0-350	8
Upconversion NPs-MnO_2	0.9	Not given	10
Carbon dots-MnO_2	0.3	1-10	14
Carbon dots-MnO_2	0.6	1-200	16
Carbon dots-MnO_2	0.022	0.2-600	17
Iridium(III) complex-MnO_2	0.13	1-200	18
CPs@MnO_2-AgNPs	0.55	0.8-80	This work